JOURNAL OF PROPULSION AND POWER
Vol. 13, No. 3, May–June 1997

Nonlinear Stability Testing of Full-Scale Tactical Motors

F. S. Blomshield,* H. B. Mathes,† J. E. Crump,† and C. A. Beiter‡
U.S. Naval Air Warfare Center, China Lake, California 93555
and
M. W. Beckstead§
Brigham Young University, Provo, Utah 84602

The U.S. Naval Air Warfare Center has participated in a program to develop an improved understanding of linear and nonlinear combustion instability in solid propellant rocket motors. One goal of this program was to develop a systematic database of motor stability data. This paper describes the nonlinear aspects of the motor firings and analysis. The motors used had diameters of 127 mm and were 1.7 m long. The majority were loaded with an 88% solids reduced-smoke ammonium perchlorate propellant with a nominal burning rate of 6.1 mm/s at 6.9 MPa. Motor pressures ranged from 3.45 to 10.34 MPa and various grain geometries were tested. In addition, motors have been fired that contain 1% 8-μm aluminum oxide, 90-μm aluminum oxide, and 3-μm zirconium carbide as stability additives in place of 1% ammonium perchlorate. This paper discusses experimental methods of motor pulsing and various theoretical approaches to predict pulse amplitudes in motors. The paper also examines nonlinear acoustic motor response to various amplitudes of acoustic pulsing and the resultant characteristics of sustained nonlinear oscillations. Finally, some theoretical interpretations are presented from the experimental motor data. The results show that there is a direct relationship between the dc pressure shift and the magnitude of the acoustic oscillations.

Introduction

THE term nonlinear as used in the context of combustion instability can describe several phenomena, including processes that lead to limit amplitudes, the presence of high-amplitude shock-fronted pressure waves, triggered instabilities, and mean pressure deviations associated with acoustic waves in a motor. Considerable attention has been paid to this form of instability in recent years because of potentially severe consequences to motor operation when it occurs.

The possibility of occurrence of a triggered instability is of particular concern to missile designers and users alike. To the user in the field, the consequences of a triggered instability can mean failure of that motor's mission. A triggered instability can occur in a motor that, without the triggering disturbance, is otherwise stable. Once triggered, the motor remains violently unstable until the end of burn. Triggering can occur from nozzle ejecta or from chamber pressure pulses induced by other means. In nonlinear instability research, ejecta or pressure pulses are deliberately introduced at predetermined times and at desired initial disturbance amplitudes as the motor burns to test the motor's response.[1–5] Reference 5 showed that the pulsed effect of ejector and pyrotechnic pulses is equivalent. In the present program, pyro pulsers rather than ejecta were utilized to create pressure pulses in the motors. A complete description of the test procedures, test matrices, and results can be found in Ref. 6. A companion paper has also been written[7] describing the linear stability results from these same motor firings.

Received Feb. 12, 1991; presented as Paper 91-1953 at the AIAA/SAE/ASME/ASEE 27th Joint Propulsion Conference, June 24–26, 1991; revision received Jan. 30, 1997; accepted for publication Feb. 1, 1997.

*Research Scientist, Research and Technology Division. Senior Member AIAA.
†Research and Technology Division (Retired).
‡Scientist, National Ground Intelligence Center, U.S. Army.
§Professor, Chemical Engineering. Associate Fellow AIAA.

The testing portion of the program involved firing 127 mm-diam motors loaded with a reduced-smoke AP/HTPB baseline propellant formulation. A number of internal motor configurations, several minor variations of the baseline propellant formulation, two motor lengths, and several mean chamber pressures have been used in the test program. The program utilized readily available hardware, but a specially designed forward closure, as well as some custom nozzle sizes, were required. Most motors were acoustically pulsed three times during burn with a variety of pulse amplitudes. The pulses were generated by pyro or blowdown pulsers of conventional design. All motors were equipped with high-frequency response pressure transducers in addition to standard ballistic pressure transducers.

The objective of pulsing motors was to test motor stability to acoustic waves. Motor response to pulsing falls into two categories: 1) the motor is stable to a pulse (i.e., acoustic waves generated by the pulse decay with time) or 2) the motor becomes violently unstable following a pulse. Stable motor response is discussed in the companion paper[7] on stability testing of full-scale tactical motors. Triggered instabilities have been under intense study and analytical techniques are available for ad hoc assessing of various aspects of this form of nonlinear motor behavior.[8–12] The objective of this paper is to present experimental results of triggered instabilities, acoustic data from pulsed motors, including methods used to pulse motors, and a discussion of relationships between linear and nonlinear instability.

Pulser Performance

Pulser Design and Components

This section will describe the pulse hardware, subscale pulser testing, comparisons of a subscale test to two distinct pulser prediction theories, and pulser testing in tactical motors. The pyro pulser used to introduce pressure pulses into motors is shown in Fig. 1. A small heavy-walled stainless-steel body is bored through and counterbored to provide for a powder chamber, an electric squib, and a method for mounting it on a motor. A squib is potted in the pulser body with room-tem-

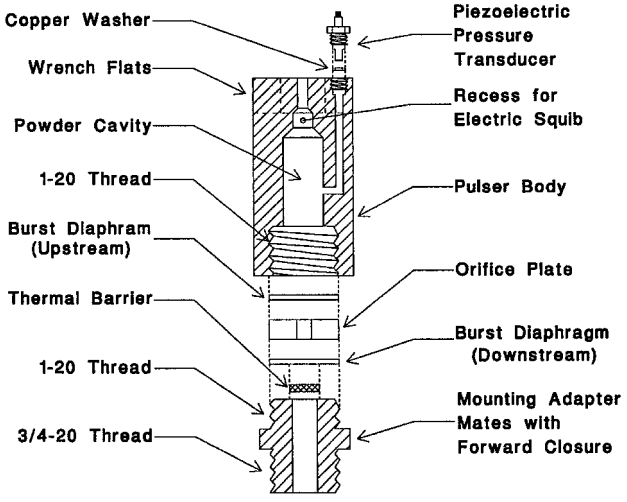

Fig. 1 Pyro pulser components.

perature vulcanizing rubber. The squib alone may provide sufficient energy for pulsing a motor or, should additional energy be needed, the squib may ignite a charge of propellant placed in the bore of the pulser body. The end of the body opposite the squib is threaded for a mounting adapter. The adapter clamps an orifice plate and one or two burst diaphragms between itself and the pulser body. The other end of the adapter threads into a hole in the forward closure of the motor. A thermal barrier is inserted into the adapter to protect the downstream diaphragm from adverse effects of exposure to hot gases in the motor. Some of the parts in the pulser were varied to suit the needs of a particular pulsing situation, as explained next.

Pulser performance varied depending on the powder charge weight used, the orifice diameter, and the placement and thickness of burst diaphragms. The powder charge, when used, was canister grade Red Dot, a double-base flake propellant commonly used in the loading of shotgun shells. Orifice plates were made of 3.175-mm-thick stainless steel. They were bored and stamped to indicate the hole diameter. Diaphragms were made of commercial half-hard brass shim stock. Tests of the shim stock, run separately from the tests of the pulsers, showed that samples of shim stock from the various packages had similar shear moduli. Thus, the burst pressure was a linear function of thickness for a given orifice diameter. A downstream diaphragm was always used in conjunction with a charge of Red Dot to seal the pulser interior from invasion by hot gases from the motor. As the program progressed, a thermal protector was placed between the downstream diaphragm and the motor to reduce the possibility of diaphragm softening because of contact with motor gas. Several thermal protection schemes were investigated. The method finally chosen was a 2.5-mm-thick disk of white polystyrene foam. The disk was a light press fit in the adapter port. It was pushed against the diaphragm as the final step in pulser assembly. The disks were of nominal 13 mm diameter. Each disk weighed about 22 mg.

The initiator was a modified Navy Mark II electric squib, which consisted of a coined copper case, a base assembly with two external lead wires, and an internal bridge wire. The source of squib energy was a 90-mg charge of 4F-G black powder mixed with $BKNO_3$ to provide a specified brisance. (The standard Mark II contains no $BKNO_3$.) Outer dimensions of the squib's body were 7.1 mm diameter and 11.4 mm length.

Subscale Pulser Testing

Prior to use in motor tests, each pulser load was evaluated in a laboratory facility using steel tubes pressurized with helium. The tubes were instrumented with pressure transducers to measure the pressure wave amplitudes generated by the pulsers. A variety of pulser load combinations was tested. Each combination of powder charge, diaphragm thickness, and arrangement were given an alphabetical load ID as shown in Table 1.

Table 1 Summary of pulser loads

Load ID	Charge weight, mg	Diaphragm thickness, mm		Orifice diameter, mm
		Upstream	Downstream	
A	0	None	None	9.02
B	100	None	0.05	2.51
C	100	None	0.20	3.66
D	200	0.20	0.20	3.66
E	100	None	0.20	5.05
F[a]	100	0.20	0.20	5.05
G	100	None	0.20	7.49
H[a]	100	0.20	0.20	7.49
I[a]	0	None	0.10	3.66
J	100	0.10	0.10	3.66
K	100	0.20	0.20	3.66
L	0	None	0.05	2.51
S	0	None	None	2.51
T	0	None	None	3.66

[a]These pulser types were not fired in motors.

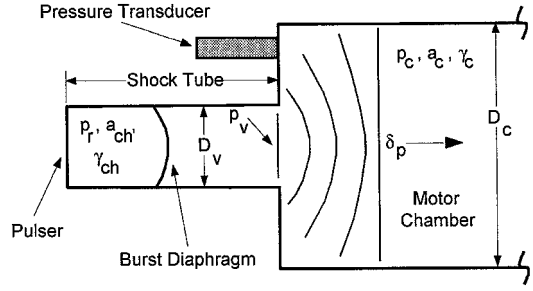

Fig. 2 Simplified schematic of pulser test setup.

The pulser laboratory tests were analyzed using two distinct theories. One is based on the classical shock-tube theory[4] and one is an empirical approach.[5] A brief description of each theory will be followed by a comparison with subscale data.

Shock-Tube Analysis

In this analysis developed by Murray et al.,[4] the pulser chamber immediately aft of the rupture diaphragm/orifice assembly is treated as a classical shock tube. The shock forms at the orifice plate, travels through the motor mounting adapter (Fig. 1), and expands in a quasispherical manner into the test chamber. Figure 2 illustrates a simplified schematic of the pulser test setup and motor cavity.

In Fig. 2, γ, a, and D are the ratio of specific heats, speed of sound, and diameters of the pulser (subscript ch) and motor chamber (subscript c), respectively. At the instant that the diaphragm bursts, the relation between the rupture pressure p_r and shock amplitude p_v is given by the classic shock-tube equation:

$$\frac{p_r}{p_c} = \frac{p_v}{p_c}\left\{1 - \frac{(\gamma_{ch}-1)(a_c/a_{ch})[(p_v/p_c)-1]}{\sqrt{2\gamma_c}\sqrt{2\gamma_c + (\gamma_c+1)[(p_v/p_c)-1]}}\right\}^{-[2\gamma_{ch}/(\gamma_{ch}-1)]} \tag{1}$$

The magnitude of the shock wave decreases as it expands in a quasispherical manner to fill the test chamber. The pulse amplitude is defined as the shock-wave amplitude once it has expanded to fill the test chamber. The wave then is characterized as a traveling planar shock wave. The effect of the quasispherical shock wave expansion is given by

$$\frac{\delta p}{p_c} = \left(\frac{p_v}{p_c} - 1\right)\sqrt{\frac{1}{1 + 1.75(D_c/D_v)^2}} \tag{2}$$

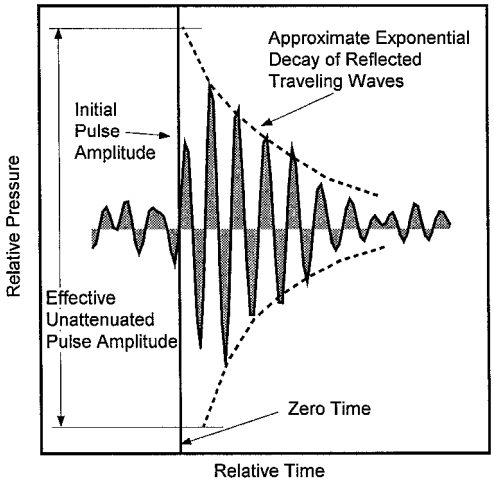

Fig. 3 Example of test record for pulser tests, transducer at head end of test chamber.

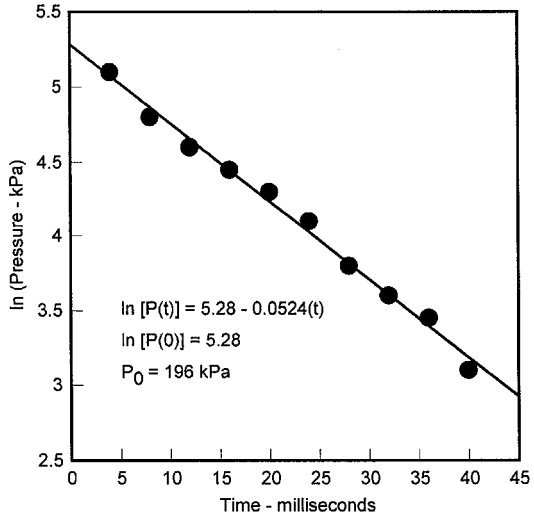

Fig. 4 Example of data reduction for pulser tests.

Thus, given the pulser and test chamber diameters, the rupture and test chamber pressures, and the necessary ratio of specific heats and speeds of sound, the effective pulser amplitude dp can be computed from Eqs. (1) and (2).

In reality, the expansion of the shock wave to fill the test chamber is a complex, three-dimensional event marked by a chaotic inflow of hot pulser gases. The organization of the shock wave into a planar traveling wave does not occur until several chamber diameters downstream. Because of this complex process, the initial pressure amplitude measured by the transducer is substantially less than the first reflection of the traveling wave. This initial amplitude can be thought of as the attenuated effective pulse amplitude. Decay of the first and subsequent reflections of the traveling wave occurs approximately in an exponential manner. Extrapolation of the exponential envelope to the initial pulse time gives an approximate value of the effective unattenuated pulse amplitude. Figure 3 shows this exponential decay and Fig. 4 shows the exponential curve fit back to zero time and an effective pulse amplitude.

Empirical Analysis

In this analysis, developed by Lovine,[5] mass and energy balance equations are applied to the combustion chamber. These take the form of two ordinary differential equations with pressure and temperature as dependent variables, and when solved simultaneously yield the amplitude of the pulse introduced into the test chamber. The pulse amplitude δp is related to the mass of pulser gases injected into the test chamber δm_p, via

$$\delta_p = \frac{\beta a_{ch}^2 \delta m_p}{g\gamma_{ch} A_c L(t_v/t_c)} \tag{3}$$

where β is a constant of proportionality, a_{ch} and γ_{ch} are the speed of sound and ratio of specific heats in the pulser, respectively; A_c and L are the test chamber cross-sectional area and length, respectively; t_v is the pulser vent time; and t_c is the time period of the test chamber's first longitudinal mode. It should be noted that in this analysis the convention of defining the pulse amplitude is the extrapolated value (as previously described) divided by 2. This factor of 2 arises from a tendency of a pressure transducer mounted normal to the direction of the traveling wave to measure nearly twice the amplitude of the actual reflected wave (see Ref. 5, pp. 39–42).

Comparison with Experiments

Table 2 lists the physical constants utilized in both analyses. Pulser loads A, S, and T (see Table 1) were omitted from the analysis because of their lack of burst diaphragms, making them inapplicable to either theory. The determination of β (empirical analysis) was determined empirically. A comparison of the experimental and predicted pulse amplitudes for both theories are shown in Figs. 5 and 6. In general, the shock-tube theory gave better agreement with experimental results than the empirical approach. Except for loads B, C, I, J, and part of the tests with load E, the majority of errors were less than $\pm 20\%$.

Adapting to Motor Conditions

The test hardware for evaluating pulser load performance provided a basis for evaluating the pulse-pressure amplitude in a test chamber of known cross-sectional area. Conditions in motors, however, involved pulser pressure waves in chambers (defined by the motor's interior) with cross-sectional areas different from the laboratory tests. The procedure for determining which pulser load was best suited to give the desired pressure amplitude in a motor at a given point in burn was as follows:

1) Pulsing times in the baseline motor (star–aft, 6.9 MPa) were initially chosen for 1, 2, and 3 s.

2) Pulsing times in other motors were based on the fractions of web burn established by the baseline motor pulsing times.

3) Pulse amplitudes were determined for each motor based on prior experience regarding susceptibility of a motor being triggered unstable. As a rule, pulse amplitudes were tailored to be progressively weaker as burn time progressed.

4) A given web burn defines a cross-sectional area in the motor chamber. That area typically differed from the area of the laboratory test apparatus in which pulsers had been initially tested. To account for the effect of cross-sectional area on pulse strength, the pulse strength desired in the motor was scaled back to the test apparatus. The scaling rule was that the pulse amplitude was inversely proportional to the cross-sectional area of the chamber.

5) When the motor pulse amplitude was scaled to an equivalent test chamber amplitude, the test data were reviewed and a pulser load chosen that came closest to the calculated test chamber amplitude. That load was used for the motor test.

The process of choosing a pulser is illustrated in Fig. 7. Of the 20 pulser load combinations tested in the laboratory, 11 were used in motors. A listing of pulse loads used on motors is shown in Table 1. Note that some of the loads consist of the initiating squib alone in association with an orifice plate. Such combinations were necessary to achieve a low-pulse amplitude for some motors. In addition, three other loads not used in motors were added to the analysis.

Table 2 Physical constants used in the pulser performance analysis

	Charge 1, 90-mg squib	Charge 2, 90-mg squib, 100-mg Red Dot	Charge 3, 90-mg squib, 200-mg Red Dot
Respective loads	I, L	B, C, E, F, G, H, J, K	D
a_{cr}, pulser gas sonic velocity, m/s	705	955	1009
R, pulser gas constant, J/kg-K	188	241	257
γ, pulser gas ratio of specific heats	1.170	1.193	1.195

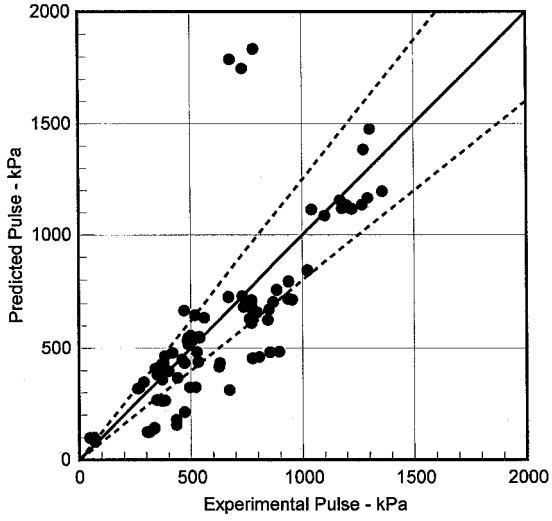

Fig. 5 Comparison of experimental and predicted pulse amplitudes, shock-tube theory with 20% error bands.[4]

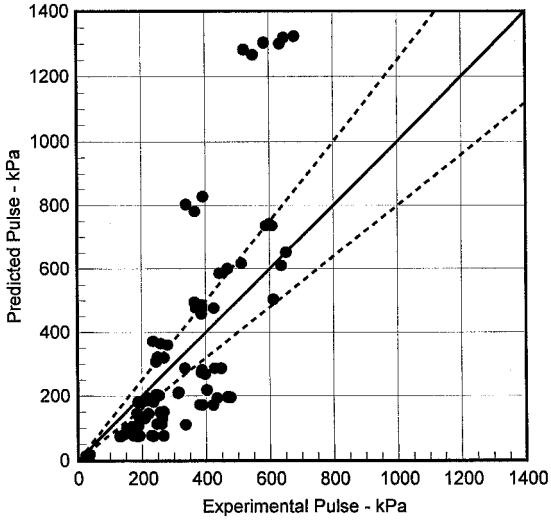

Fig. 6 Comparison of experimental and predicted pulse amplitudes, empirical theory with 20% error bands.[5]

Motor Tests

Test Matrix

Propellant was cast and case-bonded into 127-mm-diam steel motor cases. Casting was accomplished using three types of mandrels, all of which were available from other programs and adapted for use with the test motors. The mandrels were a full-length star, a partial star, and a cylinder. Two motor lengths were fabricated. Motors cast in 1.7-m-long cases oscillated at a fundamental longitudinal frequency of approximately 330 Hz. These were designated as 300-Hz motors. Most of the tests were conducted in the 300-Hz motors. Four tests used 0.85-m-long motor cases to examine behavior at higher frequency. The 0.85-m-long motors oscillated at about 660 Hz in the first longitudinal mode. Details of motor configurations are shown in Ref. 6 and the companion paper.[7] Test variables included internal geometry, chamber pressure, motor length, propellant formulation, and pulsing strength. A summary of motor types and test conditions is shown in Table 3.

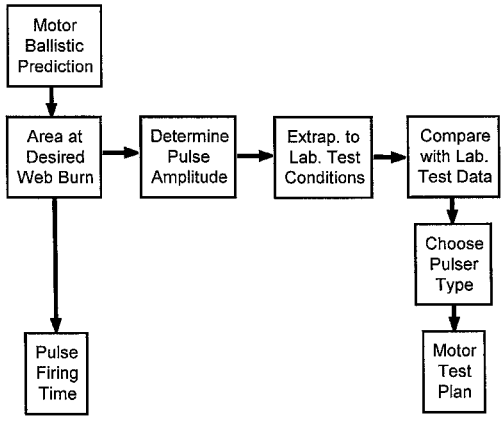

Fig. 7 Pulser selection process.

Hardware and Instrumentation

Although much of the motor hardware was adapted from available sources, the requirements for multiple pulsing and for high-frequency-response pressure transducers resulted in the design and fabrication of a special forward closure. A schematic of the forward closure and test instrumentation is shown in Fig. 8. The closure was bored and threaded to accommodate a centrally placed igniter, one standard ballistic pressure transducer, two high-frequency-response pressure transducers, and three pulsers. Test instrumentation, specially arranged for these tests, included pulse firing event channels and multichannel processing of the high-frequency pressure transducer signals.

Pulser Performance in Motors

Results of motor testing showed a variety of pulsing behaviors. Few pulse pressures measured in motors were as desired. There was a variety of causes: 1) not all planned pulse amplitudes could be matched with an appropriate load and 2) pulse timing was often different from the times that were set. The latter problem occurred mainly because of variations in motor igniter performance. In one case (motor 13) pulse times were incorrectly entered into the timer, and for motors 12 and 13 the pulsers were inadvertently interchanged. Pulser types, a comparison of pulse amplitudes, pulse times, and resulting motor stability alphas are presented in Table 4. More discussions on the measured stability alphas are presented in the companion paper on linear stability.[7]

Nonlinear Characteristics of Solid Rockets

Combustion-driven pressure oscillations, either in a rocket motor or in a laboratory device such as a T-burner, normally reach a finite limiting amplitude. The amplitude will reach this limit when nonlinear mechanisms damp oscillations more strongly than the driving mechanisms can amplify the oscillations. At the limiting pressure amplitude, the driving balances the damping and the amplitude remains essentially constant. Many rocket motors are linearly stable, but when pulsed

Table 3 Motor test matrix[a]

First longitudinal frequency, Hz	Nominal pressure, MPa	Star-aft	Star-forward	Full-star	Cylinder
300	3.4	2	——	——	1
	6.9	11[b]	1	1	1
	10.3	1	——	——	——
600	13.8	1	——	——	——
	6.9	1	1	——	1
	10.3	1	——	——	——

[a]Baseline propellant = AP/HTPB.
[b]Includes three motors with 1% additive: one each with 8-μm Al_2O_3, 3-μm ZrC, and 90-μm Al_2O_3.

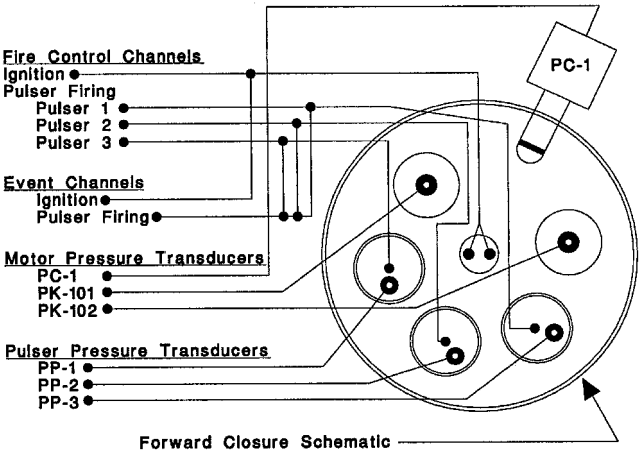

Fig. 8 Schematic of forward closure and test instrumentation.

will exhibit a nonlinear oscillation that can reach a stable limiting amplitude or can exhibit a continually growing amplitude. Various authors have developed analytical and numerical techniques for addressing nonlinear motor behavior.[8–12] This section outlines a general approach for interpreting nonlinear effects to describe aspects of nonlinear instability, such as triggering and limiting amplitudes.

The time dependence of a standing acoustic wave, $\eta(t)$ is usually described as a sinusoidal oscillation with time-dependent amplitude:

$$\eta(t) = \hat{P}(t)\sin \omega t \tag{4}$$

The time-dependent amplitude $\hat{P}(t)$ can be expanded in terms of the rate of growth of the amplitude as

$$\frac{d\hat{P}(t)}{dt} \Big/ \hat{P}(t) = \alpha + \beta\hat{P} + \gamma\hat{P}^2 \tag{5}$$

The symbol α represents the linear portion of the time-dependent amplitude, and β and γ represent second- and third-order nonlinearities, respectively. The expression has been divided by the mean amplitude for convenience.

It is informative to explore the expansion of the amplitude rate of growth expression. If only the linear term is retained, the expression reduces to the familiar expression for the linear growth rate α. If the second-order term is retained, the expression can be plotted as the rate of amplitude growth vs amplitude, yielding a linear plot such as shown in Fig. 9. Two possibilities are of interest, $\alpha > 0$ and $\alpha < 0$, where the α are the y-axis intercepts. For the system to reach a stable-limiting amplitude, the rate of growth must be zero. As shown in Fig. 9 for $\alpha > 0$, β must be less than zero to achieve a limiting amplitude and Fig. 9a is a plausible representation of a spontaneously unstable system that achieves a stable limiting amplitude. This interpretation has been used to analyze spontaneous T-burner data and make mechanistic interpretations of apparent nonlinear effects.[13] For $\alpha < 0$, β must be greater than zero to achieve a limiting amplitude, i.e., Fig. 9b. However, the limiting amplitude represents an unstable solution and is not physically realistic. For the parameters of Fig. 9b, a small pulse would trigger an instability that would never reach a limiting amplitude. Thus, a second-order system cannot represent the phenomenon of triggering.

To visualize or describe triggering, a third-order system must be considered, which when plotted as growth rate vs amplitude will result in curves such as shown in Fig. 10. Again, considering the two possibilities of $\alpha > 0$ and $\alpha < 0$, the most likely representations have been plotted. The concave downward shape ensures that the final limiting amplitude is a stable condition. If the curves were concave upward, the limiting amplitude would be unstable, which is inconsistent with experimental observation. Both Figs. 10a and 10b have similar shapes, which should be expected. Figure 10a represents a spontaneous growth rate and a stable limiting amplitude. The system represented by Fig. 10b is linearly stable, but when pulsed above a triggering amplitude, the system would stabilize at some limiting amplitude P_L. This simple logic shows that at least a third-order analysis is necessary to describe the nonlinear triggering of a linearly stable system. However, because of the similarities in Figs. 10a and 10b, the actual nonlinearities in the curves are essentially the same in spite of the different observable behavior that they each represent. Other authors have arrived at the conclusion that a third-order analysis is required to describe nonlinear triggering using a variety of approaches (numerical, analytical, etc.).[10,14]

These concepts provide one with a simple format for describing how nonlinear instability is exhibited in a rocket motor. Figure 11 shows a plot of the nonlinear growth rate for a system (or three systems) that has the same linear characteristics. At zero amplitude all three curves go through the same point ($\alpha \approx -100$). The bottom curve (a) represents a motor that would be stable to any pulse amplitude. The two upper curves [(b) and (c)] represent situations where triggering could occur. The top curve (c) is the most susceptible to pulsing (i.e., the smallest pulse would be required to trigger instability) and would result in the most violent instability or largest limiting amplitude. It is readily apparent that this mathematical representation describes the triggering phenomenon and that a very small pulse to an apparently stable system can lead to a very large limiting amplitude.

Figure 12 shows a plot of nonlinear growth rate for a typical motor with burn time as a parameter. This is characteristic of the baseline motors of this program. Curve (a) represents an early time in the firing where the motor would be stable to all pulses. This reflects the observed behavior of the motors as none of the baseline motors (at 6.9 MPa) were unstable to the initial pulse.[6,7] Curves (b), (c), and (d) represent increasing times in a firing. The margin of linear stability (i.e., the growth rate at zero amplitude) decreases in magnitude as time increases, but never reaches zero.[7] The curves represent a system that is linearly stable throughout the entire firing. However, curves (b), (c), and (d) each represent an increasingly unstable situation. Smaller and smaller pulses would be required to trigger instability in the motor, which was also characteristic of the motors in this program.[7] The curves also indicate that the limiting amplitude, characterized by the zero crossing of the amplitude scale at high amplitude, would increase with increasing time. There were not enough firings in the program to determine if this is representative of real systems or not.

Observed Trends

Limiting Amplitudes and dc Pressure Shifts

The existence of nonlinear acoustic pressure oscillations is accompanied by several phenomena that include large ampli-

Table 4 Pulser performance in motors

Motor information		Pulser		Pulse amplitude in motor chamber, kPa		Pulse fire times, s		Alpha, 1/s	
Number	Geometry/pressure	Number	Type	Planned	Measured	Planned	Actual	Growth	Decay
1	SAFT3/6.9 MPa	1	B	345	NRD[a]	1.00	——	——	——
		2	C	138	248	2.00	2.02	209	——
		3	B	69	OSC[b]	3.00	——	——	——
2	SAFT3/6.9 MPa	1	B	345	83	1.00	0.70	——	−159
		2	A	138	83	2.00	1.71	207	——
		3	B	69	OSC[b]	3.00	——	——	——
3	SAFT3/6.9 MPa	1	B	345	97	1.00	0.81	——	−112
		2	C	138	345	2.00	1.79	161	——
		3	B	69	OSC[b]	3.00	——	——	——
4	SFWD3/6.9 MPa	1	D	345	207	1.00	0.97	——	−190
		2	C	138	152	2.00	1.96	56	——
		3	B	69	OSC[b]	3.00	——	——	——
5	SAFT3/6.9 MPa	1	D	345	690	1.00	0.97	——	−176
		2	——	0	NPF[c]	——	——	——	——
		3	——	0	NPF[c]	——	——	——	——
6	SAFT3/3.4 MPa	1	D	345	124	1.00	0.76	——	−214
		2	B	138	48	2.25	2.01	——	−102
		3	B	69	41	3.25	3.01	——	−75
7	SFULL3/6.9 MPa	1	E	345	262	1.00	0.75	639	——
		2	G	138	OSC[b]	2.00	——	——	——
		3	A	69	OSC[b]	3.00	——	——	——
8a	SAFT3/6.9 MPa	1	——	0	NPF[c]	1.00	——	——	——
		2	——	0	NPF[c]	2.00	——	——	——
		3	A	69	69	3.00	3.02	134	——
8b	SAFT3/3.4 MPa	1	D	345	345	1.16	0.95	——	−210
		2	J	138	138	2.40	2.22	——	−89
		3	G	69	221	3.55	3.42	366	——
8c	SAFT3/10.3 MPa	1	C	345	138	0.85	0.62	151	——
		2	B	138	OSC[b]	1.16	——	——	——
		3	A	69	OSC[b]	2.35	——	——	——
8d				Pulses did not fire					
9	CYL3/6.9 MPa	1	K	345	138	1.00	0.75	232	——
		2	G	138	OSC	2.00	——	——	——
		3	B	69	OSC	3.00	——	——	——
10	CYL3/3.4 MPa	1	D	345	248	1.14	0.88	244	——
		2	E	138	OSC	2.32	——	——	——
		3	G	69	OSC	3.50	——	——	——
11	SAFT6/6.9 MPa	1	J	345	276	1.24	2.07	——	−143
		2	B	69	41	2.22	3.69	——	−85
		3	S	34	28	3.13	5.21	——	−60
12	SAFT6/10.3 MPa	1	T	69	83	1.03	1.37	——	−182
		2	B	69	41	1.85	2.54	——	−247[d]
		3	S	34	NRD[a]	2.64	——	——	——
13	CYL6/3.4 MPa	1	B	69	55	1.03	1.26	——	−185
		2	B	34	28	1.85	2.43	——	NRD
		3	S	34	28	2.64	3.45	——	−71
14	SFWD6/6.9 MPa	1	J	345	345	1.24	1.95	——	−201
		2	B	69	55	2.22	3.47	——	−133
		3	S	34	14	3.13	4.90	——	−33a
15[e]	SAFT3/6.9 MPa	1	K	517	1200	1.00	0.95	——	−122
		2	C	138	276	2.00	1.76	——	−84
		3	S	34	NRD[a]	3.00	——	——	——
16[e]	SAFT3/6.9 MPa	1	K	517	359	1.00	0.82	——	−232
		2	C	138	179	2.00	1.51	——	−137
		3	S	34	NRD[a]	3.00	——	——	——
17[e]	SAFT3/6.9 MPa	1	K	517	483	1.00	0.87	——	−188
		2	C	138	317	2.00	1.67	——	−75
		3	S	34	14	3.00	2.57	——	−110[d]
19	SAFT3/13.8 MPa	1	S	69	NRD[a]	0.75	——	——	——
		2	S	34	14	1.41	1.82	——	−26[d]
		3	S	34	14	2.09	2.77	——	−64[d]
20	SAFT3/6.9 MPa	1	C	276	110	1.00	0.98	——	−193
		2	B	69	28	2.00	2.17	——	−81
		3	L	0	NPF[c]	——	——	——	——
21	SAFT3/6.9 MPa	1	C	276	290	1.00	1.01	——	−251
		2	B	69	69	2.00	2.20	——	−143
		3	L	34	28	3.00	3.51	——	NRD

[a]Not reducible. [b]Oscillating. [c]No pulse fired. [d]Poor data. [e]Motors 15–17 contain 1% additive: one each with 8-μm Al_2O_3, 3-μm ZrC, and 90-μm Al_2O_3.

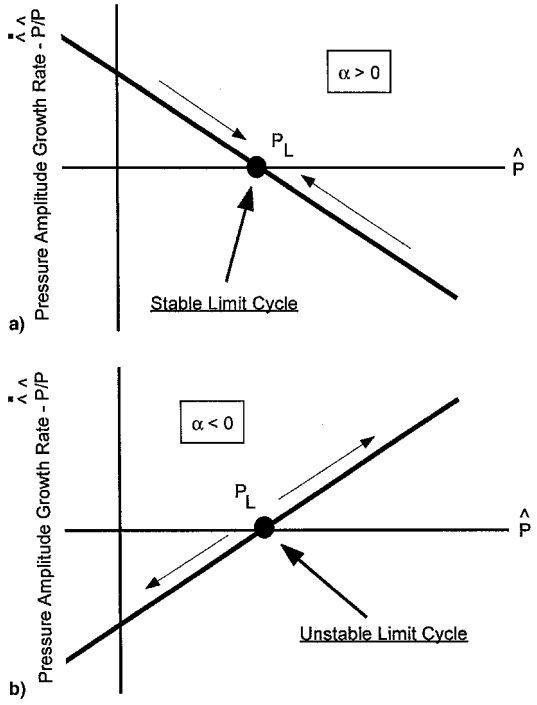

Fig. 9 Rate of growth of pressure amplitude plotted vs amplitude for a second-order system: a) $a > 0$ and b) $a < 0$.

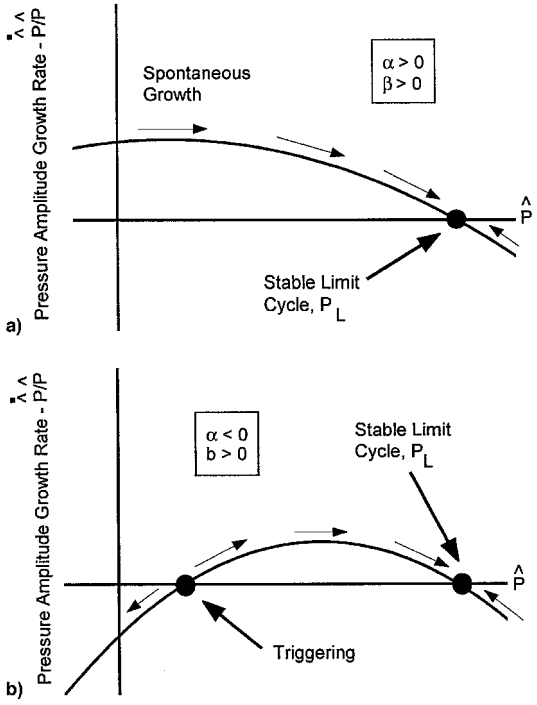

Fig. 10 Rate of growth of pressure amplitude plotted vs amplitude for a third-order system: a) $a > 0$ and b) $a < 0$.

tude sharp-fronted pressure waves and shifts in mean motor pressure. For the present discussion the following parameters are identified.

The pressure–time history of motor no. 4 that was pulsed unstable is shown in Fig. 13. The figure shows the ignition transient and two pulses: pulse 1 at ≈0.9 s that did not trigger the motor unstable, and pulse 2 at ≈1.95 s that triggered instability. This figure shows wideband data from a high-frequency response pressure transducer. The time scale covers 6 s so that individual acoustic pressure oscillations are not resolved but appear as a black band. Low-amplitude noise oscillations in the trace are visible before and after the high-amplitude acoustic oscillations. Note that following pulse 2 there was a rapid buildup of oscillation amplitude (indicated by the height of the dark band) and that there was a related upward shift of mean motor pressure (indicated by the upward shift of the band representing acoustic oscillations). The nonlinear instability parameters defined earlier were all measured at a given time after ignition. That time was chosen arbitrarily but was constant for each motor. The parameters are depicted graphically in Fig. 14 for clarity.

Nonlinear data was measured from graphical data or determined by inspection of actual data files. The value of P_{dc} was determined by inspection of motor data processed by low-pass filters. Oscillation amplitudes and dc pressure shifts are shown in Table 5. Also shown in Table 5 are the limit amplitude normalized by the initial mean motor pressure (P_{lim}/P_{s0}) and the limit amplitude normalized by the total mean motor pressure [$P_{lim}/(P_{s0} + P_{dc})$]. Data from motor no. 8b showed two distinctly different limit amplitudes.[6,7] Therefore, there are two entries for that motor in Table 5.

The dc chamber pressure shifts associated with large-amplitude acoustic waves appear to vary in proportion to the amplitude.[6,8] That relationship was investigated by plotting the dc pressure shift P_{dc} against the limiting amplitude P_{lim} as shown in Fig. 15. A linear least-squares fit was made to the data as

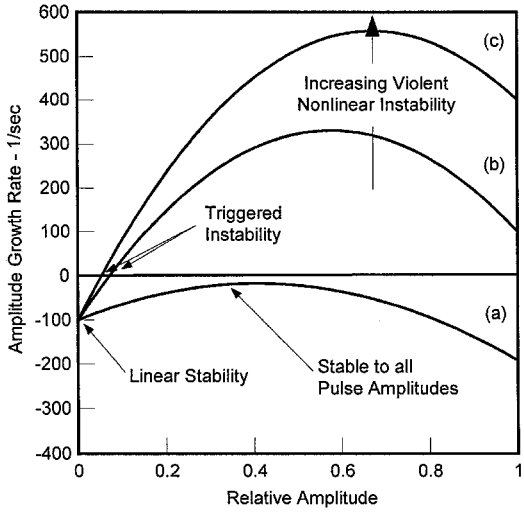

Fig. 11 Nonlinear rate of growth of pressure amplitude showing different nonlinear characteristics for the same linear stability.

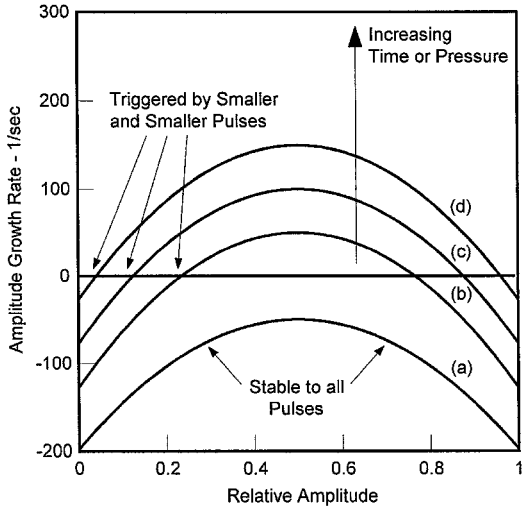

Fig. 12 Nonlinear rate of growth of pressure amplitude for a typical motor as time increases.

indicated by the line through the data points. The results show that the dc pressure shift is approximately proportional to the amplitude of the acoustic oscillations. This implies that there is a proportionality between the acoustic erosivity and the magnitude of the acoustic velocity.

Motors with Stability Additives

Solid particles are often added to reduced smoke propellants with the intent of suppressing acoustic oscillations. The principle intent with motors 15–17 was to pulse them in the same manner as the baseline motors at 6.9 MPa to see if the additives had an effect on nonlinear instability. Unfortunately, the strengths of the first pulses (18, 7, and 8%) were not, in general, comparable to the first pulses of the baseline propellant (2, 2, and 13%). These data are presented in Table 6. However, the fact that these motors remained stable to more severe pulses while weaker pulses caused the baseline motor to go unstable is significant. This suggests that stability additives play a role in nonlinear combustion instability suppression. For the second pulses, if one considers the pulse amplitudes of the second pulse in the additive motors 15, 16, and 17 (4, 4, and 6%) to be nearly comparable to the second pulse in motors 1, 2, and 3 (4, 2, and 6%), one could conclude that the additives did increase the margin of stability since the pulses in the additive motors decayed while the pulses in motors 1, 2, and 3 grew. The lower value of the response function for the higher modes for the additive propellants also[6,7] supports this conclusion, since a pulse could not as easily excite these modes into a nonlinear instability. The particle damping computed for the first longitudinal mode is very low.[6] However, the particle damping will be more effective for the higher acoustic modes and will help damp nonlinear combustion instability. For the third pulses there were no comparable data.

Effect of Pressure on Nonlinear Characteristics

Many years ago Brownlee[12] made the observation that the nonlinear susceptibility of a motor increases with increasing pressure. The results of this study support that early observation.[12] First, as was discussed in the companion paper,[7] the linear stability margin of motors decreases with increasing pressure, i.e., higher pressure motors have a smaller linear stability margin. This generalization also seems to apply in the nonlinear sense and is supported by the pulsing data. Of the 3.4-MPa motors with the star–aft grain, motor 6 was stable to all three pulses, and motor 8b was stable to the first two pulses, only becoming unstable on the third pulse. In contrast, the baseline motors with a pressure of 6.9 MPa typically were stable to the first pulse only, and unstable to the second while the high pressure motor (no. 8c at 10.3 MPa) was unstable to the first pulse. Thus, the susceptibility to nonlinear pulsing is higher at 10.3 MPa and lower at 3.4 MPa. In the cylindrical grain motors both the 6.9 and 3.4 MPa motors were unstable to the first pulse. The relative magnitude (P_{lim}/P_{so}) of the limiting amplitude reached at the different pressures for the cylindrical motors was essentially the same, 0.53 and 0.59, respectively (see Table 5). Thus, the severity of the induced

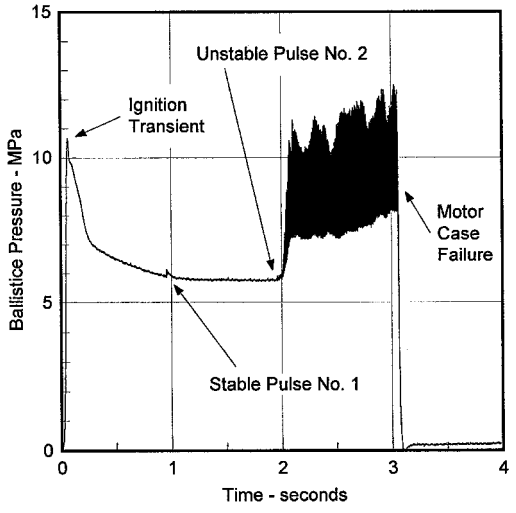

Fig. 13 Pressure–time history of a motor pulsed unstable (motor no. 4).

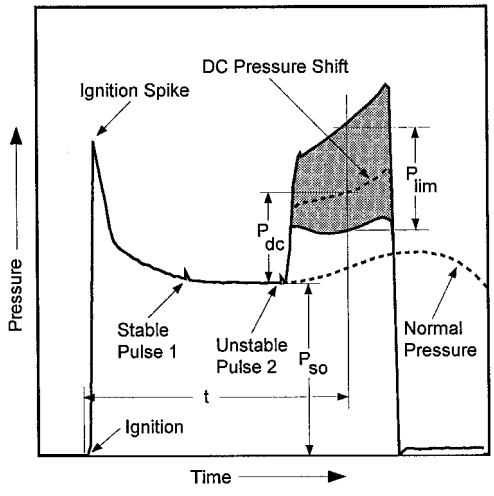

Fig. 14 Illustration of nonlinear instability parameters.

Table 5 Oscillation amplitudes and dc pressure shifts in motors pulsed into nonlinear instability

Motor information			Triggering pulse and alpha					Oscillation parameters						
Motor no.	Geometry	Nominal pressure, MPa	Pulse no.	Time, s	Pulse, kPa	Percent	α, 1/s	P_{so}[a]	P_{lim}[b]	P_{dc}[c]	P_{lim}/P_{so}	P_{dc}/P_{so}	$P_{lim}/P_{so} + P_{dc}$	Time, s
1	SAFT3	6.9	2	2.02	248	4.3	209	5.7	5.2	3.5	0.90	0.61	0.56	2.28
2	SAFT3	6.9	2	1.71	83	1.6	207	5.3	4.6	3.1	0.87	0.59	0.55	2.40
3	SAFT3	6.9	2	1.79	345	6.2	161	5.6	5.7	2.8	1.01	0.51	0.67	2.20
4	SFWD3	6.9	2	1.96	152	2.7	56	5.7	4.0	2.6	0.70	0.45	0.48	2.60
7	SFULL	6.9	1	0.75	262	3.6	639	7.3	3.8	1.8	0.52	0.25	0.42	1.50
8a	SAFT3	6.9	3	3.02	69	1.2	134	5.8	5.7	4.0	0.99	0.70	0.58	3.25
8b[d]	SAFT3	3.4	3	3.42	221	6.3	366	3.8	0.9	0.7	0.24	0.18	0.20	4.00
8b[d]	SAFT3	3.4	3	3.42	221	6.3	366	3.8	4.0	2.3	1.05	0.61	0.65	4.20
8c	SAFT3	10.3	1	0.62	138	1.6	151	8.6	7.8	6.1	0.90	0.71	0.53	1.25
9	CYL3	6.9	1	0.75	138	2.6	232	5.3	3.1	1.9	0.59	0.36	0.43	1.50
10	CYL3	3.4	1	0.88	248	6.5	244	3.8	2.0	1.6	0.53	0.43	0.37	1.75

[a]Motor chamber pressure at the time of the initiating pulse, MPa.
[b]Limit amplitude of the acoustic oscillations, MPa peak-to-peak.
[c]Shift of motor chamber pressure associated with acoustic oscillations, MPa.
[d]Motor 8b oscillated mildly and then more strongly as indicated by two sets of results.

stability seems to be independent of the mean pressure, but the susceptibility to triggering increases with increasing pressure.

The mechanism that causes the nonlinear susceptibility is somewhat questionable. However, a factor that seems to be related to the nonlinear effects is the gas velocity. The susceptibility to triggering increases and the mean velocity decreases with increasing burn time or pressure. Thus, there appears to be an inverse relationship between the velocity and triggering. Two mechanisms can be postulated as being related. First, with lower mean velocity, flow reversal is more easily achieved by a given pulse amplitude. Thus, a given pulse can more easily induce flow reversal, which will lead to an earlier onset of acoustic erosivity and the corresponding nonlinear pressure wave disturbance. A second possible mechanism is that of turbulence. A lower mean velocity means a lower Reynolds number, which has been shown to give a lower nonlinear effect in T-burners.[6,13] This could also have a contributory effect in motors.

Nonlinear Characteristics of the Combustion Response

Another factor contributing to the nonlinear nature of the system is propellant combustion.[6,14,15] To infer this contribution, one must consider the propellant response curve as a function of frequency. For illustration purposes Fig. 16 shows two curves that could correspond to two different propellants. The first six modes of a motor configuration are also indicated in the figure.

The response of propellant A is higher for the first two modes but drops off rapidly for increasing frequencies. Propellant B is slightly lower for the first two modes but continues to increase for the third, fourth, and fifth modes. For a given motor design, propellant B would have a lower margin of linear stability than propellant A for the first mode. However, in considering the nonlinear susceptibility of the two propellants, propellant B would be more susceptible to nonlinear effects than propellant A because of its higher response for the higher modes. If propellant B were subjected to a pulse (containing a wide spectrum of frequencies), the propellant would respond to the higher modes more than propellant A would. The positive reinforcement of the higher modes by propellant B would possibly sustain or amplify the pulse, whereas the lack of driving by propellant A would allow the pulse to decay. Thus, a propellant such as propellant B that has higher response at frequencies corresponding to the higher modes of a motor will be more susceptible to nonlinear effects (particularly pulsing) than a propellant that has a lower response at higher frequencies.

An example of this behavior was seen by motor firings that took place in the United Kingdom.[15] Their baseline propellant had a response lower than those reported in Refs. 6 and 7 at low frequencies and then a greater response at higher frequencies. It exhibited behavior very similar to propellant B in Fig. 16.

Thus, although the T-burner only measures the linear driving characteristics of propellants, nonlinear characteristics of a propellant can be inferred from T-burner data through proper interpretation.

Relationships Between Linear and Nonlinear Instability

The measured growth and decay alphas for the baseline star–aft motors using the baseline propellant are shown in Fig. 17 vs the pulse amplitude nondimensionalized by the chamber pressure. The solid points are decay alphas and the open points are growth alphas. The data points are keyed to the pulse number, chamber pressure of the motor, and pulse amplitude. Several observations can be made. First, it is observed that the decay alpha is essentially independent of pulse severity. This can be seen by examining the pulse 1 decay alphas for the

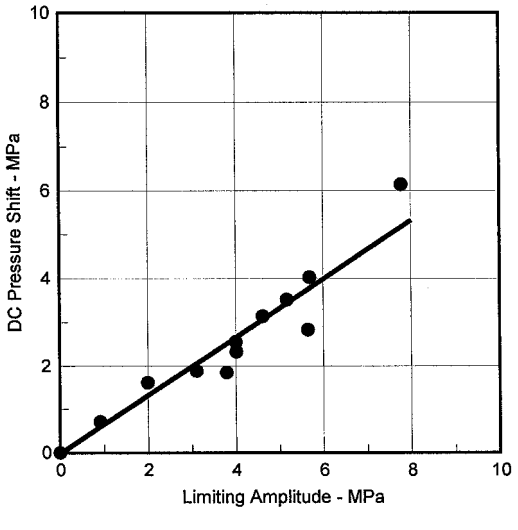

Fig. 15 DC pressure shift in nonlinearly unstable motors vs limit amplitude (data from Table 5).

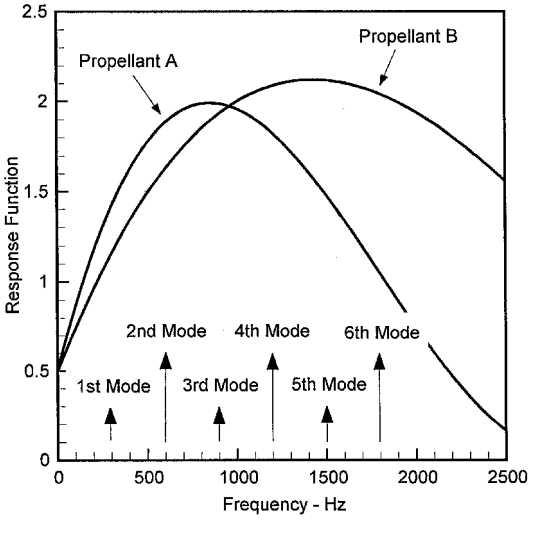

Fig. 16 Inferring nonlinear characteristics of propellants from T-burner data.

Table 6 Pulse time-amplitude-alpha comparison of baseline and additive motors

Test no.	Geometry	P_{mm} MPa	P_{av} MPa	Pulse no. 1			Pulse no. 2			Pulse no. 3		
				s	kPa[a]	α	s	kPa[a]	α	s	kPa[a]	α
1	SAFT3	6.9	5.5	NRD[b]	——	——	2.02	248	+209	OSC[c]	——	——
2	SAFT3	6.9	5.5	0.70	83	−159	1.71	83	+207	OSC	——	——
3	SAFT3	6.9	5.5	0.81	97	−112	1.79	345	+161	OSC	——	——
5	SAFT3	6.9	5.5	0.97	690	−176	NPF[d]	——	——	NPF	——	——
15	SAFT3	6.9	6.5	0.95	1200	−122	1.76	276	−84	NRD	——	——
16	SAFT3	6.9	5.0	0.82	359	−232	1.51	179	−137	NRD	——	——
17	SAFT3	6.9	5.7	0.87	483	−188	1.67	317	−75	2.57	14	−110[e]

[a]Actual pulse amplitude by extrapolated back to zero time. [b]Not reducible. [c]Oscillating. [d]No pulse fired. [e]Weak pulse motors 15–17 contain 1% additive: one each with 8-μm Al_2O_3, 3-μm ZrC, and 90-μm Al_2O_3.

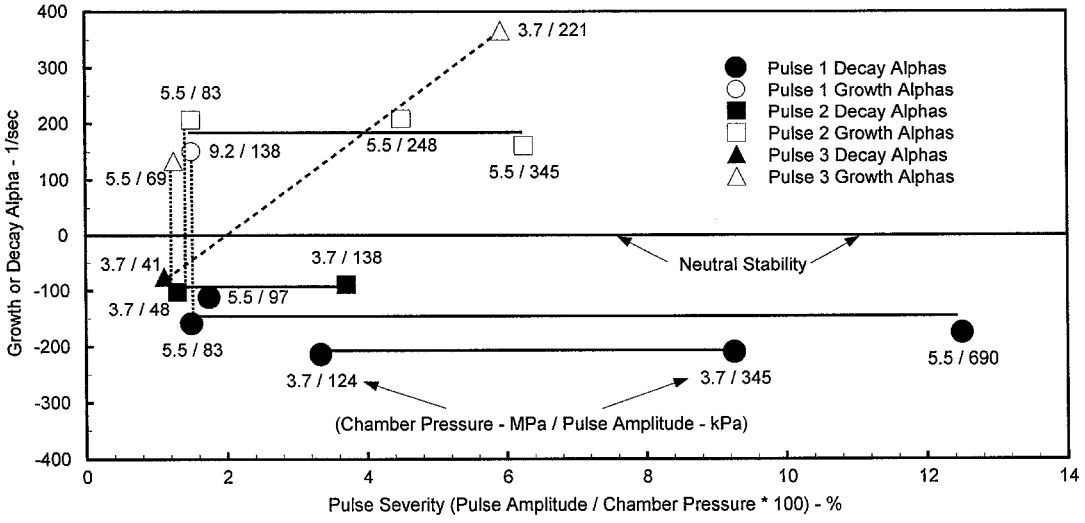

Fig. 17 Measured alphas vs pulse severity for baseline star-aft geometry for three pressures and pulses 1, 2, and 3.

motors at 5.5 MPa (solid circles). The pulses of 2, 2, and 13% resulted in decay alphas of −159, −112, and −176 reciprocal seconds, respectively, indicating that the measured decay alphas are essentially independent of pulse amplitude. This can also be seen in data at 3.7 MPa where pulse 1 values of 3 and 9% resulted in decay alphas of −214 and −210, and pulse 2 values of 1 and 4% resulted in decay alphas of −102 and −89 (solid squares). Solid lines are shown in Fig. 17 to illustrate this relationship. These observations lend credence to the comparisons of the measured decay alphas and the predicted linear decays that establish the linear stability limits described in Refs. 6 and 7.

The second observation is that the growth alphas are also essentially independent of pulse severity. This can be seen by examining the pulse 2 growth alphas for the motors at 5.5 MPa (open squares with solid line). Thus, pulses of 2, 5, and 6% resulted in growth alphas of +207, +209, and +161 reciprocal seconds, respectively. This conclusion is dependent on the data reduction method used to determine the growth alphas. The growth alphas shown in Fig. 17 are the growths for the first longitudinal acoustic mode. Although a large portion of the acoustic energy is contained in the first mode, the growth alpha as measured here may not be sufficient to draw the conclusion that the growths are independent of pulse amplitude. Physically, however, it seems reasonable to expect that the growth would depend on the motor acoustic field and the propellant combustion response to the disturbance, and not on the magnitude of the disturbance (once the disturbance exceeds the stability threshold).

The third observation is that there appears to be a correlation between mean motor pressure and the pulse amplitude required to excite nonlinear instability. Motors that were stable to a particular pulse at a low mean pressure were unstable to the same pulse (same web distance) at a higher motor pressure. Evidence to support this conclusion is shown by the dotted vertical lines in Fig. 17. The first example is a 5.5 MPa motor that was stable to the first pulse at 1.5%, 83 kPa (solid circle), and the 9.2-MPa motor, which was unstable to the first pulse at 1.5%, 138 kPa (open circle). Another example is the 3.7-MPa motor that was stable to the second pulse at 1.3%, 48 kPa (solid square), and the 5.5-MPa motor that was unstable to the second pulse at 1.5%, 83 kPa (open square). The final example is the 3.7-MPa motor that was stable to the third pulse at 1.1%, 41 kPa (solid triangle), and the 5.5-MPa motor that was unstable to the third pulse at 1.2%, 69 kPa (open triangle). These results are in agreement with the results of the linear stability predictions as functions of motor pressure that establish the linear stability limit.

Another observation from this data (Fig. 17) is that there can be a crossing of the linear stability boundary for a given pressure (in this case) by an increase in the magnitude of the pulse. The third pulse in the 3.7-MPa motors demonstrates this fact (dashed line). A 1% pulse resulted in stability (solid triangle), whereas a 6% pulse caused instability (open triangle). Unfortunately, this was the only example of this type that was obtained. If more data were available it would be possible to develop a stability map showing motor stability as a function of pressure, pulse timing, and pulse amplitude.

Summary

Motor test data obtained from 23 motors fired during the present program substantiated earlier experience, which indicated that motors would be relatively resistant to being triggered unstable early in burn time as compared to susceptibility to triggering late in burn time. The trends observed in these tests seem to follow the linear stability predictions discussed in the companion paper.[7] All of the motors were stable to a strong pulse when the linear stability alpha was large, but they were unstable to a similar pulse amplitude later in burn when the linear stability was lower. Because of the limited number of tests it was difficult to bracket the conditions for triggering nonlinear instability. An exception was the 300-Hz star–aft (SAFT3) motors at 3.4 MPa (motors 6 and 8b), in which a 1% pulse did not trigger instability, but a 6% pulse did.

Similarly, with increasing pressure, the margin of linear stability decreases[7] and the susceptibility to triggering increases (in agreement with Brownlee's early data[12]). The increased susceptibility to triggering with increased pressure or increased burn time appears to be related to a decrease in mean motor velocity. Low-velocity situations seem to enhance the susceptibility to triggering.

Motors 15–17 were fired to determine the effect of additives on nonlinear instability. The fact that all of these motors remained stable to relatively severe pulses while weaker pulses caused the baseline motor to go unstable is significant. This documents the powerful role stability additives can play in combustion instability suppression. The lower value of the response function for higher modes for the additive propellants (see companion paper[7]) supports this conclusion, since a pulse could not as easily excite these higher modes into a nonlinear instability.[7] Also, the additives will produce particle damping that will be more effective, especially for the higher modes, than for a propellant without additives.

The data in this program suggest that susceptibility to triggering is influenced by the interior geometry of the motor. For example, tests on the 300-Hz full–star (motor 7) and on the

motors with cylindrical perforations (motors 9 and 10) showed those motors to be more susceptible to triggering than any of the other 300-Hz configurations. Both of these types of motors had constant cross sections and were symmetric front to back. Motors 7, 9, and 10 all went unstable on the first pulse with 262-, 138-, and 248-kPa pulses. Other 300-Hz configurations successfully withstood first pulse amplitudes in the range of 83–690 kPa.

This program also allowed the opportunity to evaluate pulsers and various design tools to estimate pulse amplitudes. Both shock tube and empirical theories were compared to laboratory pulse data with results, usually within 20% for the shock-tube theory.

The dc shifts in the chamber pressure, caused by acoustic wave action on propellant burning rate, are linearly proportional to the acoustic amplitude.

Data of the type presented here carry a strong message both to motor designers and users. Triggered instabilities are of more than academic interest. Standard ballistic testing will seldom reveal how susceptible a motor is to nonlinear instability. The phenomenon is capable of ruining motor performance when it occurs. The results obtained in the present test series re-emphasize the importance of testing motor stability by pulsing in addition to performing the usual stability calculations. Pulsing should be an integral part of motor qualification programs. Otherwise, it is difficult to assess the range of motor conditions (including debris discharged through the nozzle) under which a motor will remain stable. The results of this program suggest that ignorance of a motor's sensitivity to pulsing may not be a wise policy, as it has been demonstrated that a relatively minor pulse amplitude can drastically alter motor behavior.

Acknowledgments

This paper was sponsored by the Air Launched Weaponry Technology Block Office under the authority of Tom Loftus, Code 474T60D, U.S. Naval Air Warfare Center, Weapons Division, China Lake, California.

References

[1]Beck, W. H., and Jolley, W. H., "Harmonic Analysis of Piston and Pyrotechnic Pulsers for T-Burners," *Journal of Propulsion and Power*, Vol. 4, No. 3, 1988, pp. 283–285.

[2]Brown, R. S., "Blowdown Pulser Criteria for Solid Propellant Rockets," *Journal of Propulsion and Power*, Vol. 2, No. 2, 1986, pp. 110–116.

[3]Lovine, R. L., Baum, J. D., and Levine, J. N., "Ejecta Pulsing of Subscale Solid Propellant Rocket Motors," *AIAA Journal*, Vol. 23, No. 3, 1985, pp. 416–423.

[4]Murray, J. A., Condon, J. A., and Krusch, D. E., "Pulsing Criteria for Solid Rocket Motors Volume II: Motor Pulsing Design Manual," Air Force Rocket Propulsion Lab., TR-79-45, Edwards AFB, CA, March 1981.

[5]Lovine, R. L., "Nonlinear Stability for Tactical Motors, Volume IV—Pulsing Considerations Parts 1 and 2," Air Force Rocket Propulsion Lab., TR-84-017, Edwards AFB, CA, Aug. 1985.

[6]Blomshield, F. S., Crump, J. E., Mathes, H. B., and Beckstead, M. W., "Stability Testing and Pulsing of Full Scale Tactical Motors. Part 1. Final Report," U.S. Naval Air Warfare Center, WPNS TP 8060, July 1993.

[7]Blomshield, F. S., Crump, J. E., Mathes, H. B., and Stalnaker, R. A., "Stability Testing of Full-Scale Tactical Motors," *Journal of Propulsion and Power*, Vol. 13, No. 3, 1997, pp. 349–355.

[8]Baum, J. D., Levine, J. N., and Lovine, R. L., "Pulsed Instability in Rocket Motors: A Comparison Between Predictions and Experiments," *Journal of Propulsion and Power*, Vol. 4, No. 4, 1988, pp. 308–316.

[9]Hackett, R. M., "Analytical Model of Pulsing of Solid Propellant Rocket Motors," *Journal of Spacecraft and Rockets*, Vol. 22, No. 2, 1985, pp. 201–210.

[10]Baum, J. D., Levine, J. N., and Lovine, R. L., "Pulse-Triggered Instability in Solid Rocket Motors," *AIAA Journal*, Vol. 22, No. 10, 1984, pp. 1413–1419.

[11]Baum, J. D., and Levine, J. N., "Modeling Of Nonlinear Longitudinal Instabilities in Solid Rocket Motors," *Acta Astronautica*, Vol. 13, Nos. 6-7, 1984, pp. 339–348.

[12]Brownlee, W. G., "Non-Linear Axial Combustion Instability in Solid Propellant Motors," *AIAA Journal*, Vol. 2, No. 2, 1964, pp. 275–284.

[13]Jensen, R. C., and Beckstead, M. W., "Limiting Amplitude Analysis," Hercules, Inc., Air Force Rocket Propulsion Lab., TR-73-61, Magna, UT, July 1973.

[14]Lovine, R. L., and Micheli, P. L., "Nonlinear Stability for Tactical Motors, Volume I—Program Summary," Aerojet Tactical Systems, AFRPL-TR-85-017, Sacramento, CA, 1985; also Vols. II–V.

[15]Blomshield, F. S., Jolley, W. H., Harris, P. G., and Tandy, I. F. S. "The Technical Cooperation Program Technical Panel W-4: Propulsion Technology, KTA-11: Pulsed Non-Linear Combustion Instability," Vols. I–VI, Naval Weapons Center, The Technical Cooperation Program Final Rept., China Lake, CA, Oct. 1991.